01 Dec 1982

# Nonlinear Anelasticity Of Magnesium

Alexander Aning

Tetsuro Suzuki
*Missouri University of Science and Technology*

Manfred Wuttig
*Missouri University of Science and Technology*



## Recommended Citation

A. Aning et al., "Nonlinear Anelasticity Of Magnesium," *Journal of Applied Physics*, vol. 53, no. 10, pp. 6797 - 6808, American Institute of Physics, Dec 1982.
The definitive version is available at https://doi.org/10.1063/1.330068

RESEARCH ARTICLE | OCTOBER 01 1982

# Nonlinear anelasticity of magnesium

Alexander Aning; Tetsuro Suzuki; Manfred Wuttig



*Journal of Applied Physics* 53, 6797–6808 (1982)
https://doi.org/10.1063/1.330068

# Nonlinear anelasticity of magnesium

Alexander Aning
*Department of Metallurgical Engineering, University of Missouri-Rolla, Rolla, Missouri 65401*

Tetsuro Suzuki
*Institute of Applied Physics, Tsukuba University, Sakura, Ibaraki, 305, Japan*

Manfred Wuttig
*Department of Metallurgical Engineering, University of Missouri-Rolla, Rolla, Missouri 65401*

(Received 11 February 1982; accepted for publication 8 June 1982)

An approximate solution of the equation of motion of a nonlinear anelastic reed at or near resonance is presented. The steady state solution reproduces the well-known nonlinear resonances. The solution also predicts the existence of automodulations, i.e., self-excited modulations of the amplitude and phase at constant power of excitation of the reed. Numerical examples of such automodulations are presented for an antisymmetric deformation potential. Experimental studies of finite amplitude oscillations of a magnesium reed vibrating at 72 and 431 Hz at room temperature confirm the existence of automodulations. The experimental results can be semiquantitatively described in terms of the solution given. The assumption that finite deformation by twinning represents the essential nonlinearity leads to a self-consistent interpretation. The relaxation time of twinning is obtained from the analysis of the automodulation and is 22 msec in the sample investigated. It is proposed that point defects control the relaxation process.

PACS numbers: 62.20.Fe, 62.40. + i

## I. INTRODUCTION

Anelastic studies have yielded a significant insight into the properties of metals and alloys. The contributions of this branch of physical metallurgy encompass the fields of diffusion,[1] radiation damage,[2] regular alloys,[3] plastic deformation, and the study of point defects as an end in itself.[4] The major conceptual limitation of most anelastic studies is that the interpretation of the data has ultimately been based on the model of a linear anelastic solid as originally proposed by Zener[5] and extended by Nowick.[6–8] This model restricts the validity of all statements derived from anelastic studies to small or infinitesimal strains, $\epsilon \ll 1$. Although this is not serious in many cases, it does pose a problem whenever strains occur that are finite.[9,10] This is the case in twinning and first-order phase transformations in which finite strains are essential.

This paper addresses itself to dynamical twinning. The concept of nonlinear anelasticity is used to derive an approximate equation of motion of a reed in which twinning can take place. The experimental results of anelastic studies at finite amplitudes in magnesium will be presented and it will be shown that they can be understood in terms of the derived equations.

## II. NONLINEAR ANELASTICITY

The concept of nonlinear anelasticity has been introduced previously.[11] An approximate solution of the equation of motion of a nonlinear anelastic reed pertaining to a symmetrical deformation potential has been presented as well.[12] The model will be reviewed briefly in this section. Subsequently, the solution of the equation of motion will be extended to include antisymmetric deformation potentials.

The properties of the nonlinear anelastic solid may be explored by extending the known stress-strain relationship of the linear anelastic solid

$$\sigma + \tau\dot{\sigma} = C_{r2}\epsilon + C_{u2}\tau\dot{\epsilon} \tag{1}$$

to finite strains

$$\sigma + \tau\dot{\sigma} = C_r(\epsilon)\epsilon + C_u(\epsilon)\tau\dot{\epsilon}, \tag{2}$$

where

$$C_r(\epsilon) = C_{r2} + C_{r3}\epsilon + C_{r4}\epsilon^2 + C_{r5}\epsilon^3 + C_{r6}\epsilon^4, \tag{2a}$$

$$C_u(\epsilon) = C_{u2} + 2C_{u3}\epsilon + 3C_{u4}\epsilon^2 + 4C_{u5}\epsilon^3 + 5C_{u6}\epsilon^4. \tag{2b}$$

In Eqs. (1) and (2) the quantities $C_{ri}$ and $C_{ui}$ denote the relaxed and unrelaxed deformation parameters of order $i$. The relaxation time of the process giving rise to the anelasticity is $\tau$. The term deformation parameter is preferred over elastic constant as the latter refers strictly only to an infinitesimal deformation near equilibrium.

The equation of motion of a nonlinear anelastic specimen can be derived by combining its stress-strain relationship, Eq. (12), with the equation of motion

$$\rho\partial^2\epsilon/\partial t^2 = \partial^2\sigma/\partial z^2, \tag{3}$$

where $\rho$ denotes the density of the sample. In view of the fact that this equation will be used to describe nonlinear phenomena, the quantity $\epsilon$ should be understood to represent, strictly speaking, the deformation gradient. Furthermore, it must be understood that the stress and strain in Eq. (3) are both of the same type.

The combination of Eqs. (2) and (3) yields

$$\tau\rho\partial^3\epsilon/\partial t^3 + \rho\partial^2\epsilon/\partial t^2 = \partial^2[C_r(\epsilon)\epsilon]/\partial z^2 + \partial^3[C_u(\epsilon)\epsilon]/\partial z^2\partial t. \tag{4}$$

An approximate equation of motion of a clamped-free reed-like specimen follows from Eq. (4) by separating the variables



 0021-8979/82/106797-12$02.40  

$z$ and $t$. The flexural oscillations of this reed are approximated by[13]

$$\epsilon(z,t)\approx x(t)[1-\cos(\pi z/2l)], \tag{5}$$

where $l$ is the length of the reed.

The combination of Eqs. (2a), (2b), (4), and (5) gives the desired equation of motion of the fundamental mode of the reed:

$$\begin{aligned}\tau\dddot{x}+\ddot{x}+\omega_0^2[1+2C_{r3}x+(15/4)C_{r4}x^2+7C_{r5}x^3\\ +(131/8)C_{r6}x^4]\,x+\omega_0^2\tau[C_{u2}+4C_{u3}x\\ +(45/4)C_{u4}x^2+28C_{u5}x^3+(655/8)C_{u6}x^4]\,\dot{x}\\ =E\sin(\omega_1 t)+E'\sin[(1/2)\omega_1 t],\end{aligned} \tag{6}$$

where

$$\omega_0^2=\pi^2C_{r2}(4l^2\rho)^{-1}.$$

All deformation parameters are given in units of $C_{r2}$. In Eq. (6) the terms on the right have been added to represent the external excitation. Since twinning occurs at a finite strain, $E$ must be finite. The term $E'\sin[(1/2)\omega_1 t]$ represents the indirect excitation of the half harmonic due to twinning. It will be discussed more fully later.

In order to solve Eq. (6) by a perturbation method, it must be transformed so that the external excitation appears as a small perturbation. This is achieved through the transformation

$$x(t)=y(t)+b\sin(\omega_1 t), \tag{7}$$

where

$$b=E/(\omega_0^2-\omega_1^2).$$

The resulting differential equation reads

$$\tau\dddot{y}+\ddot{y}+\omega_0^2\,y=\mu f(y,\dot{y},t),\quad \mu f\ll 1. \tag{8}$$

The function $f(y,\dot{y},t)$ represents all terms except $\tau\dddot{y}$, $\ddot{y}$, and $\omega_0^2\,y$ resulting from the transformation. The solution of this equation by the method of Bogoliubov and Mitropolsky[14] is based on the premise that the term $\mu f$ results in a small correction to the well known solution of Eq. (8) for $f=0$,

$$y(t)=a\cos(\omega_1 t+\theta), \tag{9}$$

in which the amplitude $a$ and phase $\theta$ are constants. Since the term $\mu f$ represents a small perturbation, an approximate solution of the form

$$y(t)=a(t)\cos[\omega_1 t+\theta(t)] \tag{10}$$

is sought. The functions $a(t)$ and $\omega(t)$ are almost constants, i.e., slowly varying functions of time. To first order, the second and third time derivatives of $y(t)$ may thus be reduced to

$$\begin{aligned}\ddot{y}&=-2\dot{a}\omega_1\sin\Psi-(a\omega_1^2+2a\omega_1\dot{\theta})\cos\Psi,\\ \dddot{y}&=(3a\omega_1^2\dot{\theta}+a\omega_1^3)\sin\Psi-3\dot{a}\omega_1^2\cos\Psi,\end{aligned} \tag{11}$$

where

$$\Psi=\omega_1 t+\theta(t).$$

Substitution of Eqs. (10) and (11) into Eq. (8) yields

$$\begin{aligned}&(-2\dot{a}\omega_1+3a\omega_1^2\tau\dot{\theta}+a\omega_1^3\tau)\sin\Psi\\ &+(-3\dot{a}\omega_1^2\tau-2a\omega_1\dot{\theta}+a\Delta)\cos\Psi=\mu f(y,\dot{y},t),\end{aligned} \tag{12}$$

where

$$\Delta=\omega_0^2-\omega_1^2.$$

Differential equations for the amplitude $a$ and phase $\theta$ are now obtained by comparing the coefficients of $\sin\Psi$ and $\cos\Psi$ in Eq. (12) with the appropriate Fourier coefficients of $f(y,\dot{y},t)$. A lengthy but straightforward calculation yields Eqs. (13) and (14) for the fundamental resonance of the reed,

$$\begin{aligned}2\dot{\theta}/\omega_0=\{[(1-\omega_1^2/\omega_0^2)(2+3(\omega_0\tau)^2\\ +2\theta_1-3a_1(\omega_0\tau)^2]\\ +[2\theta_2-3a_2(\omega_0\tau)^2]\sin\theta\\ +[2\theta_3-3a_3](\omega_0\tau)\cos\theta\}/[4+9(\omega_0\tau)^2]\end{aligned} \tag{13}$$

and

$$\begin{aligned}2\dot{a}/\omega_0 a=\{[(1-\omega_1^2/\omega_0^2)+2a_1+3\theta_1](\omega_0\tau)^2\\ +[2a_2+3\theta_2](\omega_0\tau)\sin\theta\\ +[2a_3+3\theta_3(\omega_0\tau)^2]\cos\theta\}/[4+9(\omega_0\tau)^2].\end{aligned} \tag{14}$$

Harmonics of the phase are neglected. The functions $a_i$ and $\theta_i$ are polynomials in $a$, $b$, and $E'$. They are given in Appendix A.

The response of a nonlinear anelastic reed to a finite periodic excitation near resonance can now be discussed. Just as for a linear oscillator, the response is characterized by the resonance curve of the reed. If for constant excitation at any one frequency near resonance the amplitude and phase are constant, the resonance is characterized by the steady state conditions[14]

$$\dot{a}=\dot{\theta}=0. \tag{15}$$

These conditions in conjunction with Eqs. (13) and (14) lead to the resonance characteristic[14]

$$\nu=[1+B/A\pm(B^2/A^2-C/A)^{1/2}]^{1/2}, \tag{16}$$

where the expressions for $A$, $B$, and $C$ are given in Appendix B.

Examples of resonant response together with typical deformation potentials are shown in Figs. 1–4. Figures 1 and 2 serve merely as a check of the approach and the performance of the computer routine. It can be seen that the well-

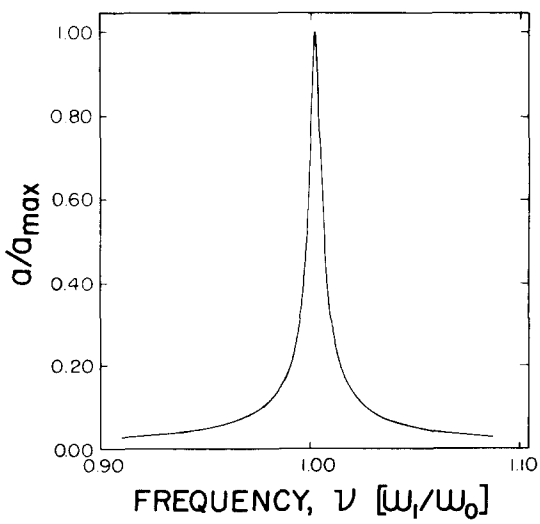


FIG. 1. Resonance curve of a linear oscillator obtained from Eq. (16) by setting all deformation parameters, except $C_{u2}$ and $C_{r2}$, equal to zero.

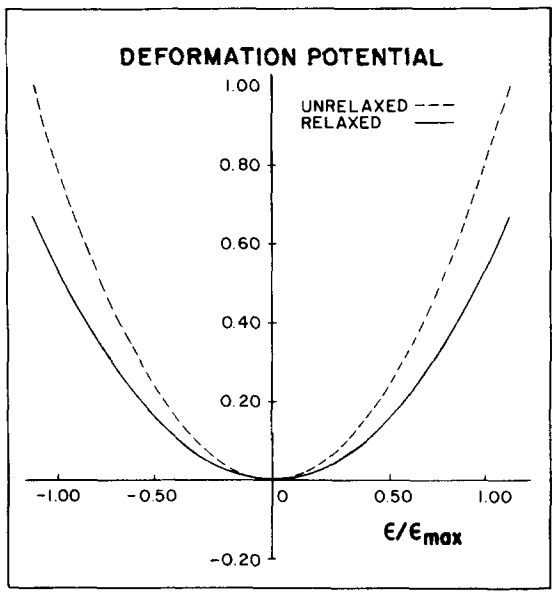


FIG. 2. Relaxed and unrelaxed parabolic symmetrical deformation potential, $F = \int C(\epsilon) d\epsilon$, obtained by setting all deformation parameters, except $C_{u2}$ and $C_{r2}$, equal to zero.

known resonance of a linear oscillator is obtained for a parabolic deformation potential. A nonlinear resonance curve characteristic of an antisymmetrical deformation potential is shown in Figs. 3 and 4. The deformation parameters in Fig. 4 are characteristic of homogeneous twinning. The parameters in Fig. 3 have been selected so that the resonance resembles the experimental data. It can be seen that negative values of $C_{u3}$ and $C_{r3}$ lead to a soft resonance as expected.

While a linear oscillator displays only the steady state in which $\dot{a} = \dot{\theta} = 0$, this is not necessarily so for a nonlinear oscillator. The phenomenon of automodulation can set in. This phenomenon is said to occur whenever the amplitude and/or phase vary periodically with time, even though the driving force is constant. There are two types of automodulations.

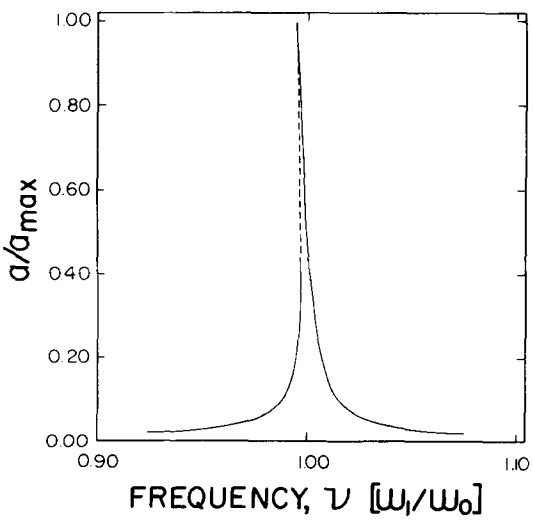


FIG. 3. A nonlinear resonance curve whose nonlinearities are due to an antisymmetrical deformation. No automodulation exists with this resonance. The dashed line represents an unstable branch.

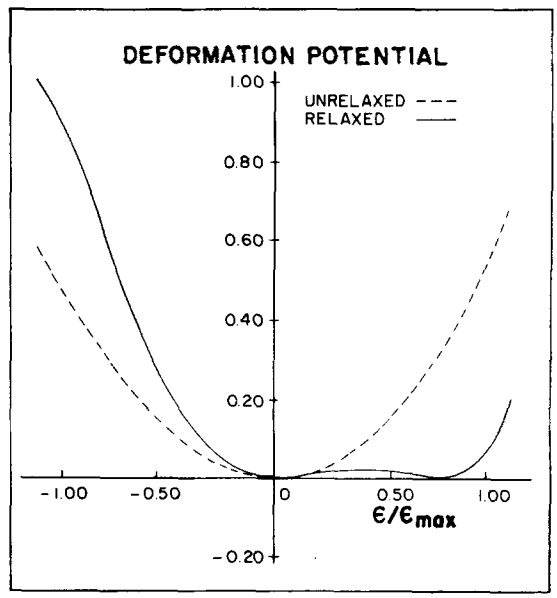


FIG. 4. An example of a relaxed and unrelaxed antisymmetrical deformation potential. The reversal of the relative magnitude of the relaxed and unrelaxed deformations indicates that no nonlinear deformation process operates at such deformations.

The Type I automodulation is described as follows: If the deformation parameters $C_{u3}$ and $C_{r3}$ are negative, the damping term in Eq. (6) can become negative at finite amplitudes. In this case, self-excitation of the reed at its eigenfre-

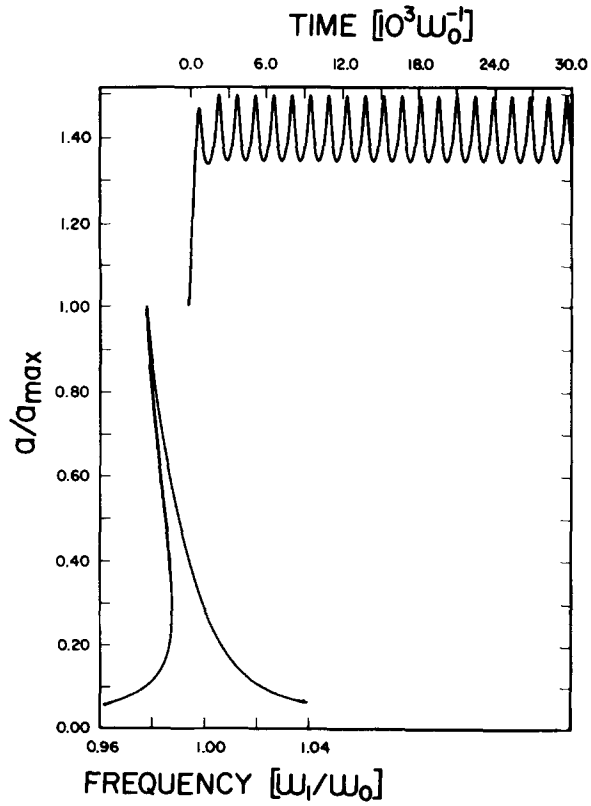


FIG. 5. A nonlinear resonance curve whose nonlinearities are due to antisymmetrical deformation and which gives rise to self-induced modulation (Type I), and the associated automodulation of the amplitude. The values of the deformation parameters and other constants are: $C_{u2} = 1.005$, $C_{r2} = 1.000$, $a_{max} = 2.356$; $C_{u3} = -0.0125$, $C_{r3} = -0.0150$, $\omega\tau = 10$; $C_{u5} = 0.00014$, $C_{r5} = 0.00014$, $B = 2.5$, $E' = 0.1$.

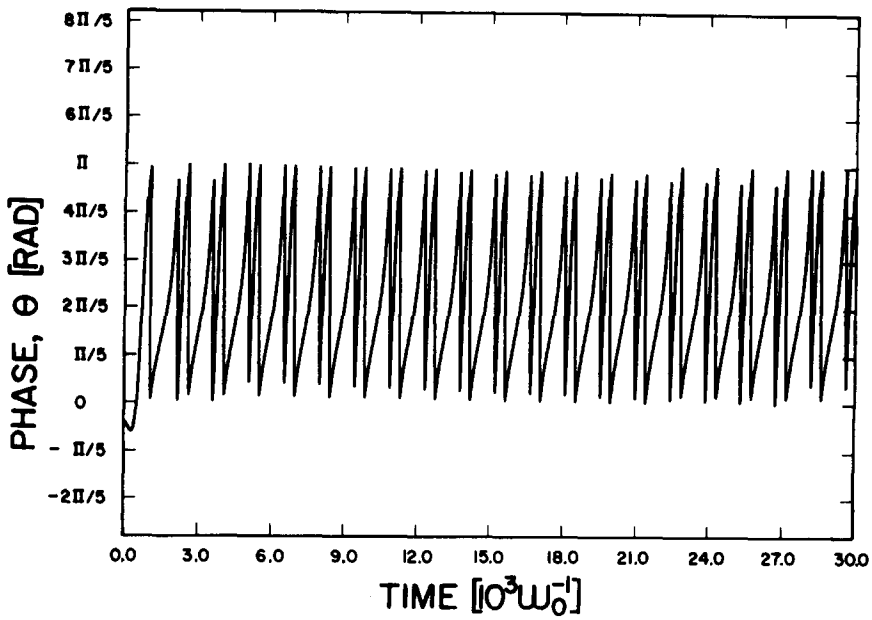


FIG. 6. Phaseautomodulation of Type I corresponding to the modulation of amplitude described in Fig. 5. The phase changes continuously [see Eq. (17)]. Here it is reset to zero after every $\pi$.

quency can exist. If this happens, the superposition of the externally excited (heteroperiodic) oscillation of frequency $\omega_1$ and self-excited (autoperiodic) oscillation of frequency $\omega_0$ gives rise to a beat of frequency $(1/2)|(\omega_1 - \omega_0)|$. This situation becomes more clear when Eqs. (13) and (14) are examined. The terms $a_i$ and $\theta_i$ are polynomials and can all become negligibly small at a certain finite amplitude. Equations (13) and (14) may be integrated to give

$$\theta = [1 - (\omega_1/\omega_0)^2]\omega_0 t, \tag{17}$$

and

$$a = a_0 + f(\sin\theta, \cos\theta). \tag{18}$$

It follows from Eqs. (17) and (18) that the beat manifests itself by a constant rate of change of the phase and an automodulation of the amplitude. Computed examples of this Type I automodulation, together with the corresponding resonance curve, are shown in Figs. 5 and 6.

In order to discuss the Type II automodulations, Eqs. (13) and (14) are rewritten as

$$\dot{\theta} = G(a,\theta), \tag{19}$$

and

$$\dot{a} = F(a,\theta). \tag{20}$$

Again, automodulation is said to occur whenever the phase and amplitude vary periodically with time around the steady state value $\theta_0$ and $a_0$, i.e.,

$$\theta = \theta_0 + \delta\theta \tag{21}$$

and

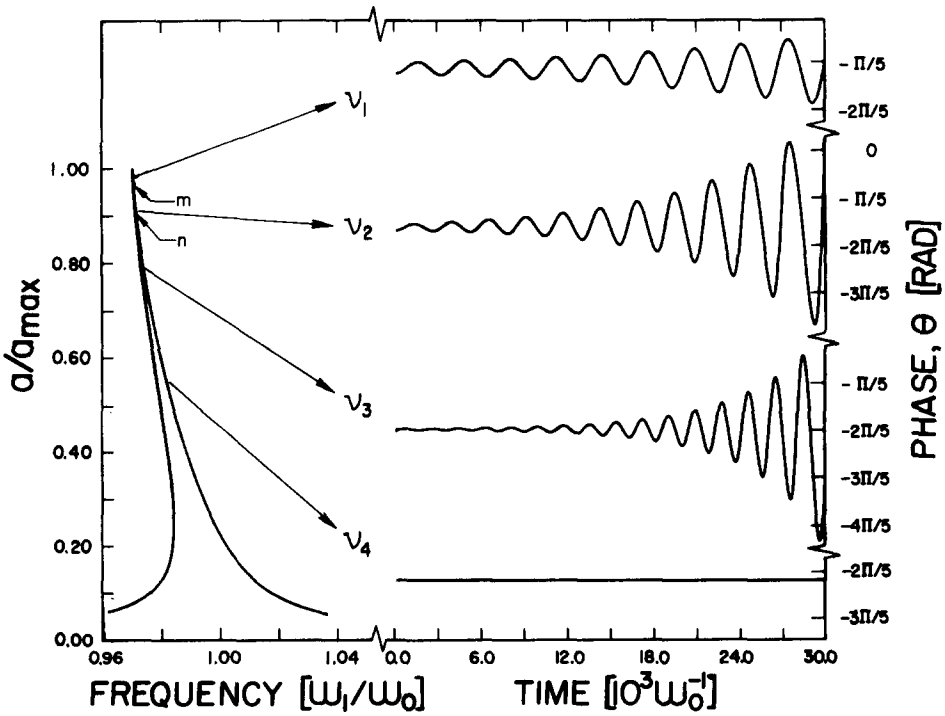


FIG. 7. Phaseautomodulations of Type II at various drive frequencies and the associated resonance curve. The deformation parameters and other constants are: $C_{u2} = 1.005$, $C_{r2} = 1.000$, $a_{max} = 2.784$; $C_{u3} = -0.015$, $C_{r3} = -0.025$, $\omega\tau = 10$; $C_{u5} = 0.00014$, $C_{r5} = 0.00014$, $B = 2.75$, $E' = 0.10$.

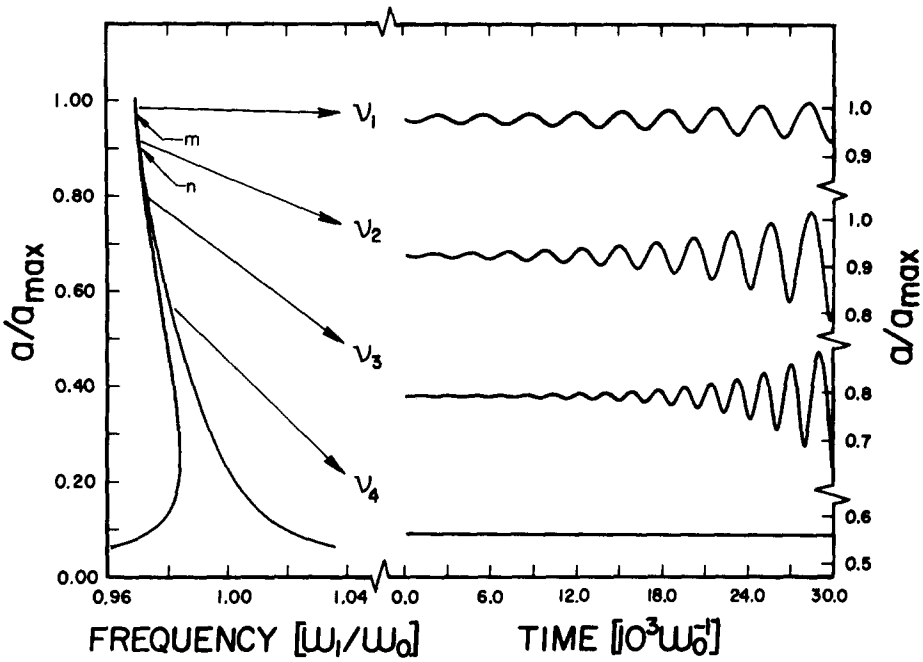


FIG. 8. Automodulations of the amplitude (Type II) corresponding to phaseautomodulations shown in Fig. 7.

$$a = a_0 + \delta a. \tag{22}$$

In the simplest case, $\delta\theta$ and $\delta a$ vary sinusoidally in time in which case their time variation is given by a differential equation[15]

$$\ddot{\delta a} - (F_a + G_\theta)\dot{\delta a} + (F_a G_\theta - G_a F_\theta)\delta a = 0, \tag{23}$$

where the subscripts denote partial derivatives.

Automodulation represents undamped oscillation of the amplitude and phase. This occurs whenever $F_a = -G_\theta$, in which case the modulation frequency is given by

$$\omega_m^2 = -(F_a^2 + G_a F_\theta). \tag{24}$$

For a linear oscillator, $F_a = G_a = 0$, and no automodulation will occur. Furthermore, the condition $F_a = -G_\theta$ is very restrictive indicating that even in nonlinear oscillators automodulations do not always occur. Computed examples of the Type II automodulation in phase and amplitude are shown in Figs. 7 and 8.

The two types of automodulation may be summarized as follows: In Type I, the phase varies linearly with time and the amplitude is modulated periodically. Both the phase and amplitude are modulated periodically in Type II. However, as indicated above, the condition for Type II is restrictive. Extended long term phase and amplitude automodulations of Type II are shown in Fig. 9. It is possible that Type II transfers to Type I after a very long time. Examples of this situation are shown in Figs. 10 and 12 for the phase, and Figs. 11 and 13 for the amplitude.

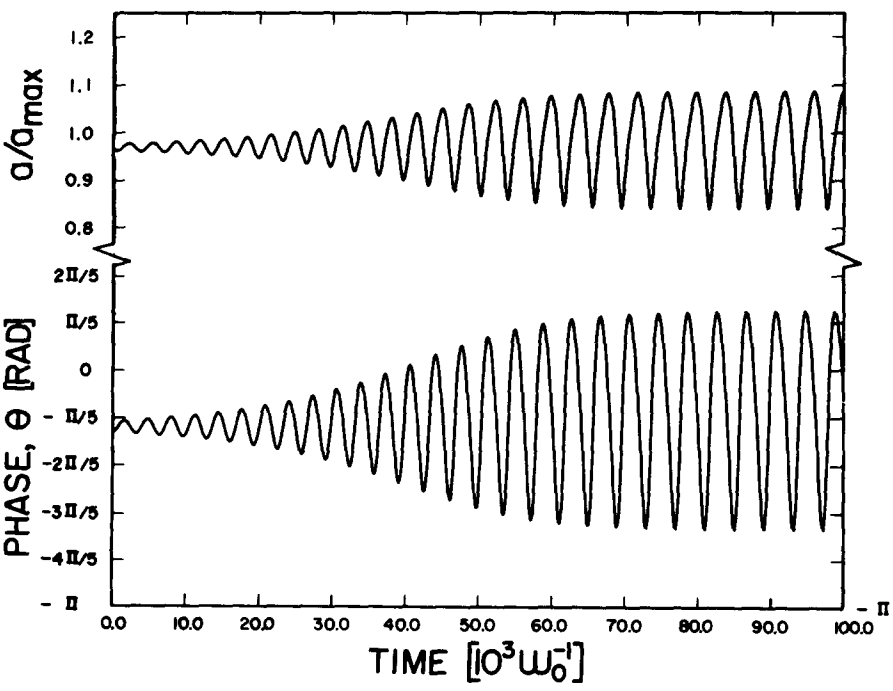


FIG. 9. Theoretical long-time phase and amplitude automodulation of Type II occurring at the drive frequency of $\nu_1$ (within the region between the point marked $m$ and the resonance tip) as shown in Figs. 7 and 8.

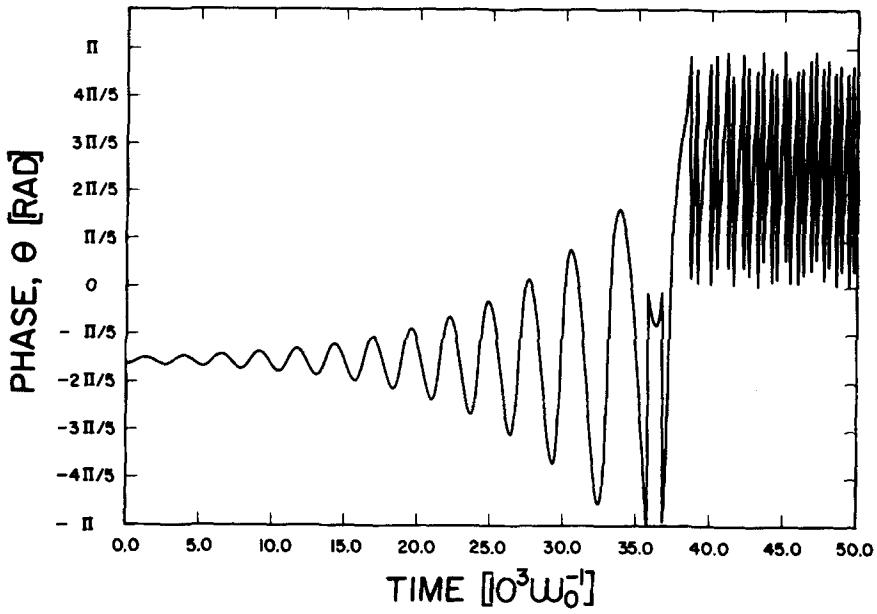


FIG. 10. Theoretical long-time phaseautomodulation at a drive frequency in the region between the points marked $m$ and $n$ as shown in Fig. 7. In this case after the transfer to Type I at $3.8\times10^{4}\omega_0^{-1}$ the phase is displayed as in Fig. 6.

## III. EXPERIMENTAL PROCEDURE AND RESULTS

A schematic of the experimental apparatus is shown in Fig. 14. The apparatus was set up in an evacuated and temperature controlled environment on a vibration isolated platform. The oscillation of the reed was excited through the force which the constant gradient Helmoltz coils shown in Fig. 14 exerted on the Sm-Co magnet clamped onto the sample.

The plane of the 99.9% magnesium reed was cut in a [214] direction with the direction of vibration being [$\bar{7}91$]. The dimensions of the two reeds investigated were 3.17 cm long, 0.635 cm wide, 0.071 cm thick, and 3.17 cm long, 0.071 cm wide, and 0.114 cm thick. Together with the mass of the Sm-Co magnet they resulted in eigenfrequencies of 72 and 431.4 Hz. Both reeds were chemically polished before starting the internal friction experiment to remove any surface damage.

Resonance curves as well as automodulation amplitude and phase time behavior were recorded on analog recorders. The data reported in this paper have been redrawn from these recordings.

Figures 15 and 16 are typical of the main results of this study. They represent a steady state resonance curve recorded with an $\omega$ sweep commensurate with the response time of the electronics and the automodulations. The automodulations were recorded by selecting a suitable drive frequency $\nu$ and waiting until they developed. The transient time for the establishment of the automodulation could be as long as several hours, and they also depended on the way in which the automodulation was started. Since an investigation of these transients was not the main goal of this study no effort was made to control them. The data shown in Figs. 15 and 16 were recorded after the automodulation amplitude was built up to about 80% of its estimated final value. It can be seen

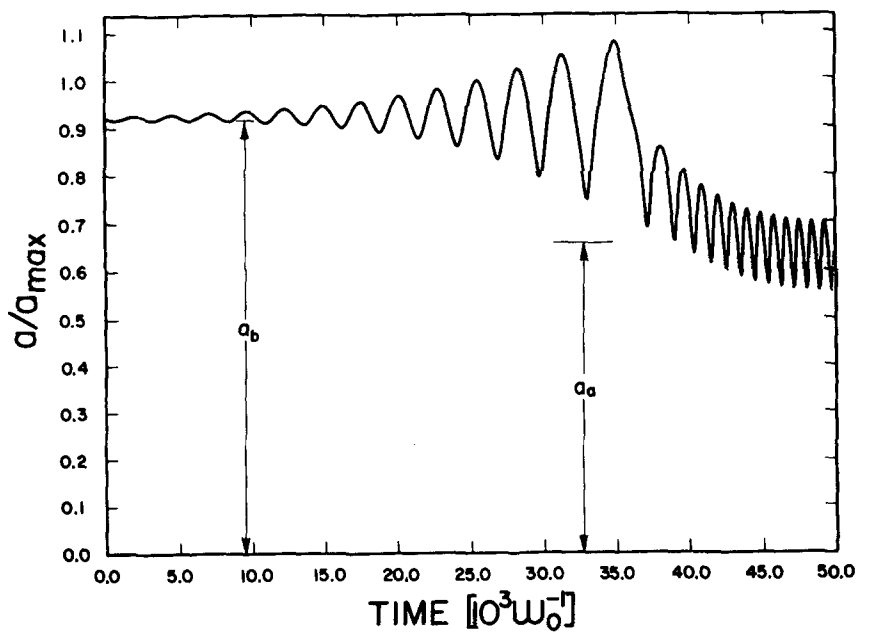


FIG. 11. Theoretical long-time amplitude automoduation at a drive frequency in the region between the points marked $m$ and $n$ as shown in Fig. 8, corresponding to the phaseautomodulation shown in Fig. 10.

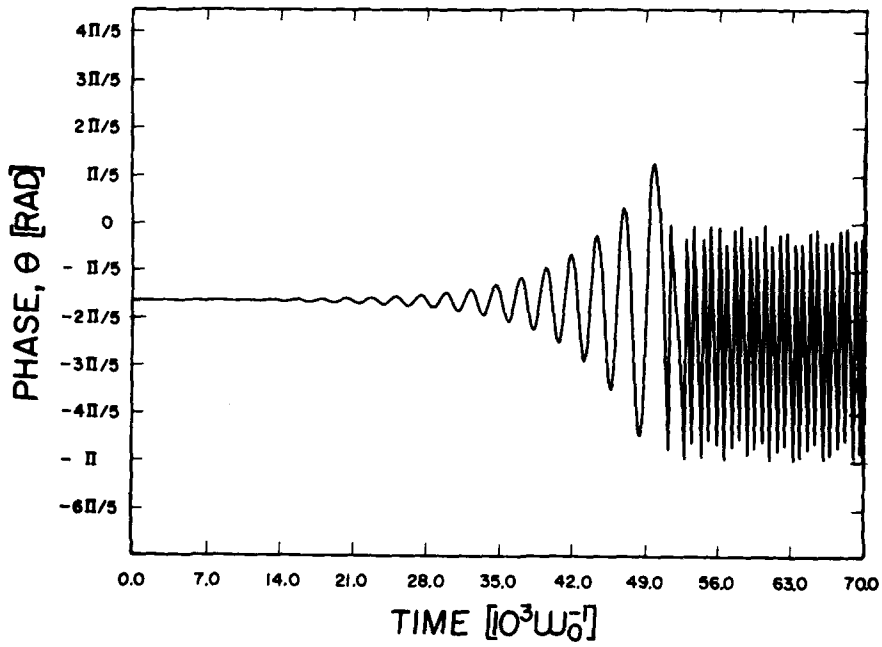


FIG. 12. Theoretical long-time phaseautomodulation at a drive frequency in the region between the points marked $n$ and $\nu_4$ as shown in Fig. 7. The phase is displayed as in Fig. 10.

that no steady state was reached. This was true even if the automodulations were allowed to take place for a very long time, as can be seen from Fig. 17. It should be explained that the automodulation data were reproducible in the sense that the same automodulation was observed at an equivalent position of the resonance curve. The resonance curves themselves shifted slightly, as can be seen from Fig. 18. The shift recovered overnight, however, if the sample was left at rest.

## IV. DISCUSSION

The data collected in the course of this study are significant in two respects. Firstly, they serve as a formal example for the model presented of the nonlinear anelastic solid. Secondly, the data contain information about the process of twinning. Both aspects will be discussed in the following.

### A. Formal aspects

The data shown in Figs. 15 and 16 can be interpreted in terms of the theory presented above. Resonance curves and the automodulation of the phase and amplitude have been calculated on the basis of Eq. (16) and Appendix A, Sec. I for various sets of relaxed and unrelaxed deformation parameters and different values of the normalized relaxation time $\omega_0\tau$. The numerical computations show that a self-consistent fit of both the resonance and automodulation data is not possible if symmetrical deformation potentials only are considered. The data, however, can be fit if it is assumed that the linear contributions are symmetrical and nonlinearities contribute exclusively to the antisymmetrical mode. A detailed fit has been achieved by systematically varying the deformation parameters characteristic of the antisymmetrical defor-

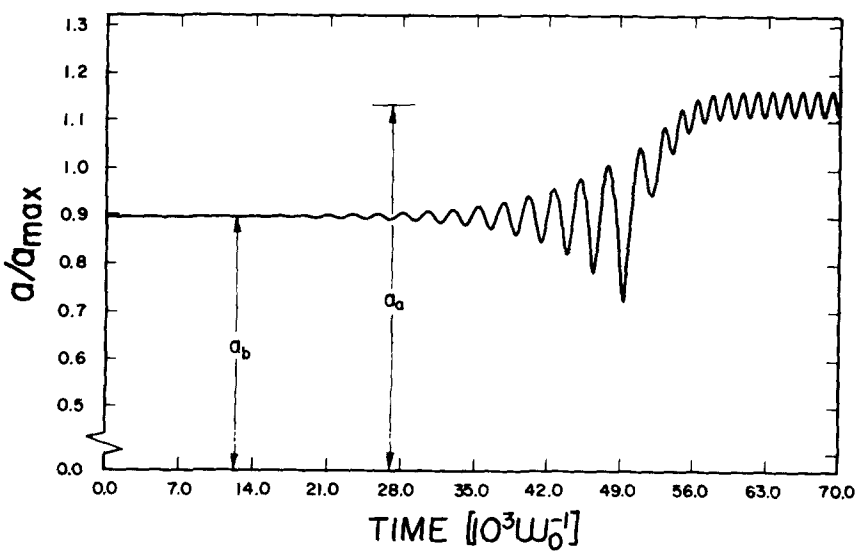


FIG. 13. Theoretical long-time amplitude automodulation at a drive frequency in the region between the points marked $n$ and $\nu_4$ as shown in Fig. 8, corresponding to the phaseautomodulation shown in Fig. 12.

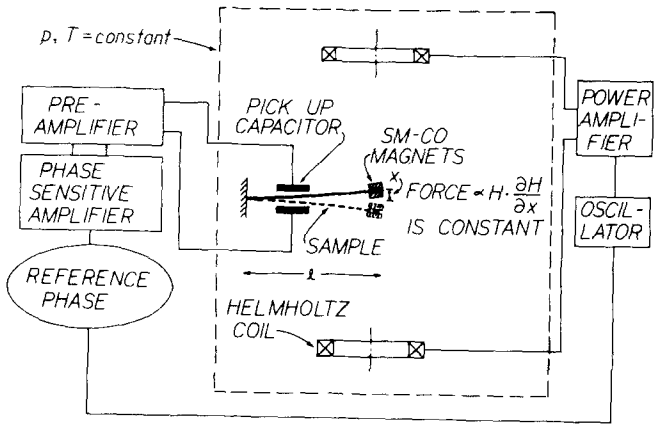


FIG. 14. Schematic internal friction apparatus used to demonstrate the simultaneous automodulation of the phase and amplitude.

mation potential until the resonance curve could be reasonably modelled. Of all the sets of deformation parameters which could model the resonance, only the set which could also model the automodulation data was considered representative of the sample. The numerical data presented in Figs. 7 and 8 were arrived at in this fashion. An antisymmetrical deformation potential is characteristic of twinning as will be shown below.

A comparison of the experimental data (Figs. 15 and 16) with the data calculated on the basis of an antisymmetrical nonlinear anelastic solid shows that the theory reproduces the experiment semiquantitatively. The agreement is strongest for the resonance curve and the frequency of the automodulation $\nu_m$ and does not extend to the amplitude of the automodulation. Furthermore, it is confined to a small range of the driving frequencies $\nu$ with respect to the long time behavior of the automodulation. The transients apparent in the computer simulation of the automodulation have been observed experimentally in all cases. An example is shown in Fig. 17. This figure shows that the automodulation amplitude and frequency reach a steady state at very long times of the order $10^9\omega_0^{-1}$. The experimental transient is an order of magnitude longer than the transient resulting from the model and shown in Fig. 9. Further, the two differ in their harmonic content. The large difference in the length of the transient is thought to be caused by metallurgical changes and will be discussed below. It should be pointed out that the experimental automodulation frequencies plotted in Fig. 19 have been determined at a time of the order of $10^5\omega_0^{-1}$, where harmonics were not yet evident. They are thus comparable to the predictions of the model. The difference in harmonic content is expected, since higher harmonics in the phase have been neglected in the calculations leading to Figs. 7–13. Their inclusion would have unduly extended the already time consuming computations.

All experimentally observed automodulations are of Type II as are the theoretically calculated ones in the frequency range from the point marked $n$ to the tip of the resonance shown in Figs. 7 and 8. Outside this frequency range the theoretically computed automodulations are of a mixed type as can be seen in Figs. 10–13. It is believed that the reason for this discrepancy has to do with the fact that the present model of a nonlinear anelastic solid describes a homogeneous deformation while the flexural vibration of the reed of finite thickness lead to an inhomogeneous deformation pattern. Automodulations of the type described by Eqs. (13) and (14) develop in a thin layer off the central axis of the reed characterized by a given amplitude of vibration $a$. In such a layer they cannot transform from Type I to Type II: The average amplitude, after transition from Type II to Type I, designated as $a_a$ in Figs. 11 and 13, decreases with increasing the average amplitude before the transition, labelled $a_b$ in the same figures, as the computer calculations show. The

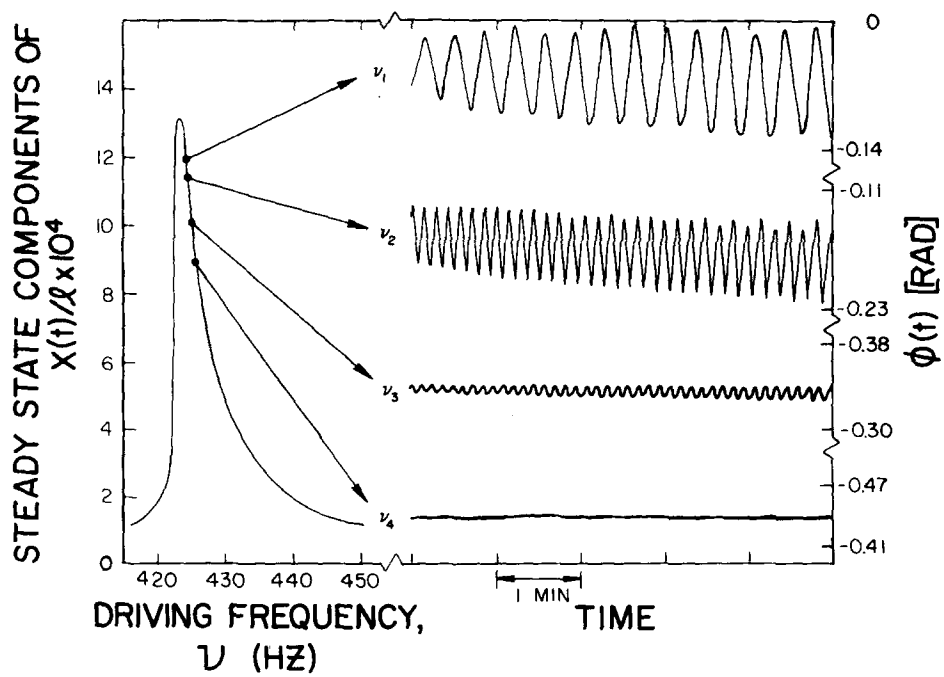


FIG. 15. Experimental phaseautomodulation at various drive frequencies together with the resonance curve that gave rise to the automodulation. The eigenfrequency of the reed was 431.4 Hz.

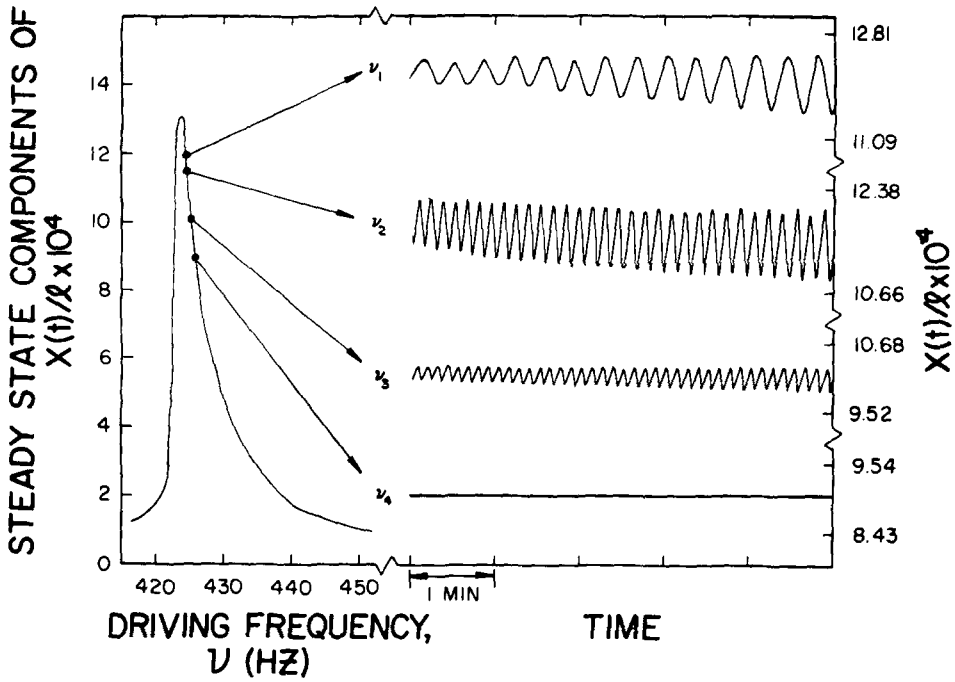


FIG. 16. Experimental amplitude automodulation corresponding to the phaseautomodulation in Fig. 15.

resulting large interlayer stresses resulting from the amplitude reversal evident by comparing Figs. 11 and 13 must be expected to inhibit the development of true self-excited oscillation in the reed, and hence quench automodulations of Type I. This argument leads again to the conclusion that only those automodulations can develop which will have a compatible amplitude dependence. Such is the case for the Type II automodulations. Since they are also the ones observed experimentally, Type I auto-oscillations will be excluded from further considerations.

The frequency dependence of Type II automodulations is shown in Fig. 19. Again, it can be seen that the experimentally determined values agree semiquantitatively with the computer data for the reed with resonance frequency of 72 Hz (Fig. 19). The set of deformation parameters which reproduces the 72 Hz data does not, however, reproduce the automodulation frequency at the higher frequency of 431.4 Hz (Fig. 20). This discrepancy is attributed to the different thickness to length ratio of the two reeds. The reed with the higher resonance frequency has a larger thickness to length ratio. Therefore, the nonlinear character of the oscillations will result in different effective amplitudes of vibration for the two different reeds. Hence they cannot be described by the same set of average deformation parameters. In viewing Figs. 19 and 20 it should also be recalled that the automodulation frequency depends on the amplitude of automodulation, as does a nonlinear oscillation. After the automodulation has developed to about 80% this variation is minor.

Finally, the difference between the experimental resonance curve in Fig. 18 and the one computed on the basis of Eq. (16) and Appendix A, Sec. I (Fig. 7) requires comment. The two differ mainly in the shape of the tip of the curves. It

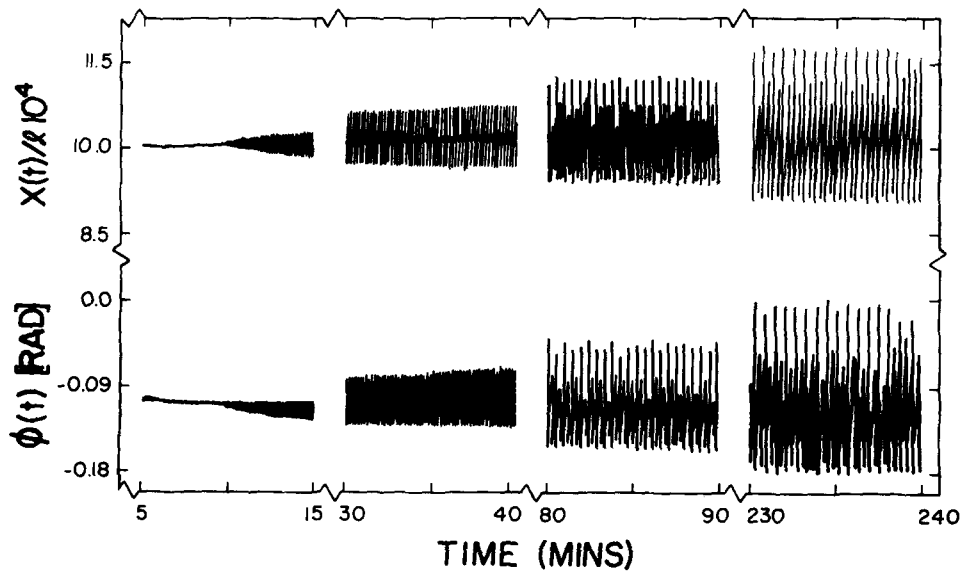


FIG. 17. Experimental long-time simultaneous phaseautomodulation and amplitude automodulation. The eigenfrequency of the reed was 431.4 Hz.

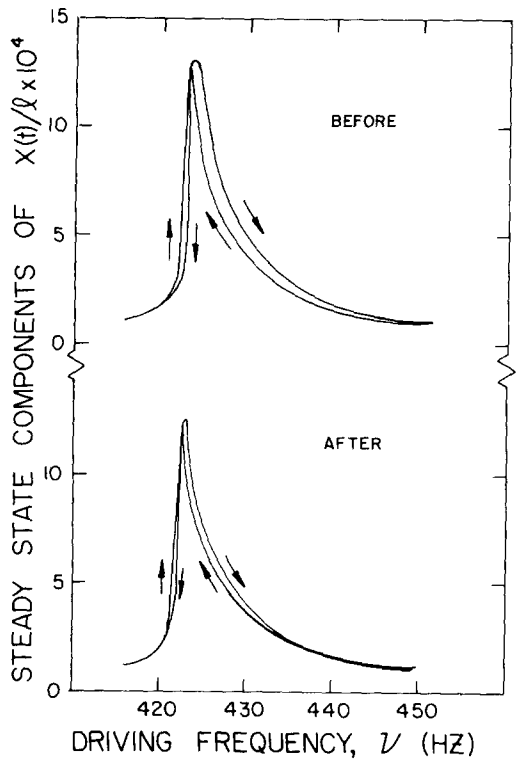


FIG. 18. Resonance curves drawn before and after 3 h of taking automodulation data at an eigenfrequency of 431.4 Hz.

is blunted in the experimental case while sharp in the computer model. A blunted tip can arise in two ways. First, the resonance curve of the reed of finite thickness can be considered to be the superposition of the resonance curves of its layers which will give rise to a convoluted resonance curve with a blunted tip. Second, the twinning process itself can commence at different stress levels which will have the same effect. These and other more metallurgical aspects will be discussed in the following section.

### B. Metallurgical aspects

Automodulation phenomena have now been observed in the course of internal friction studies of Mg,[16] Zn,[17,18]

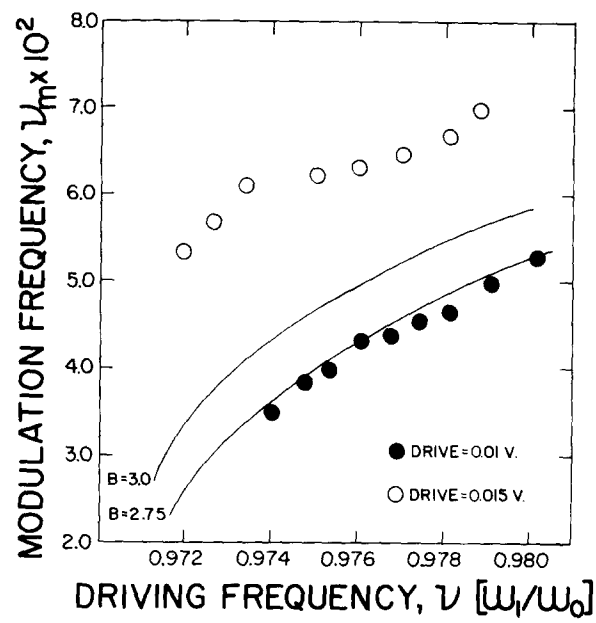


FIG. 19. The theoretical and experimentally observed automodulation frequency $\nu_m$ as a function of drive frequency $\nu$, at an eigenfrequency of 72 Hz.

Zr,[19] Cu-Al-Ni,[12] Cu,[20] and Cu-Al-Zn.[21] All these metals and alloys have in common is that they deform by twinning or by transforming martensitically. Therefore, it is suggested that the present data be interpreted in terms of twinning. Twinning, as shown in Fig. 21, is a polar deformation process[22] in the sense that a reversal of the stress cannot operate the same twinning system. It must, therefore, be described by an antisymmetrical deformation potential as shown in Fig. 4. In the course of the oscillation of the reed, twinning occurs only every second time the reed is deflected from its equilibrium position. This means that twinning occurs at half the frequency with which the reed oscillates, and is the reason for including the subharmonic excitation of order 1/2 into Eq. (6). The half harmonic can only arise in the Fourier transform of the function $f$ in Eq. (8) if the deformation parameters characteristic of an antisymmetrical deforma-

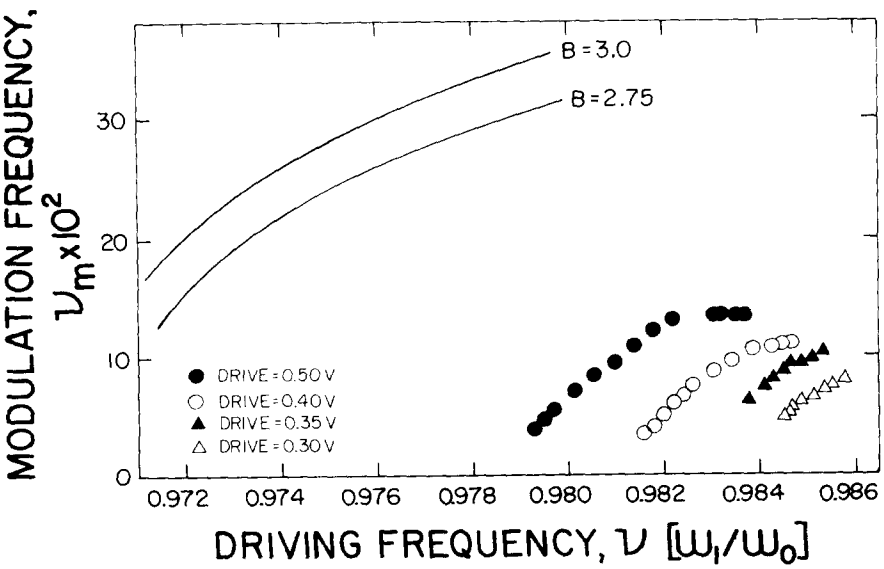


FIG. 20. The theoretical and experimentally observed automodulation frequency $\nu_m$ as a function of drive frequency $\nu$, at an eigenfrequency of 431.4 Hz.

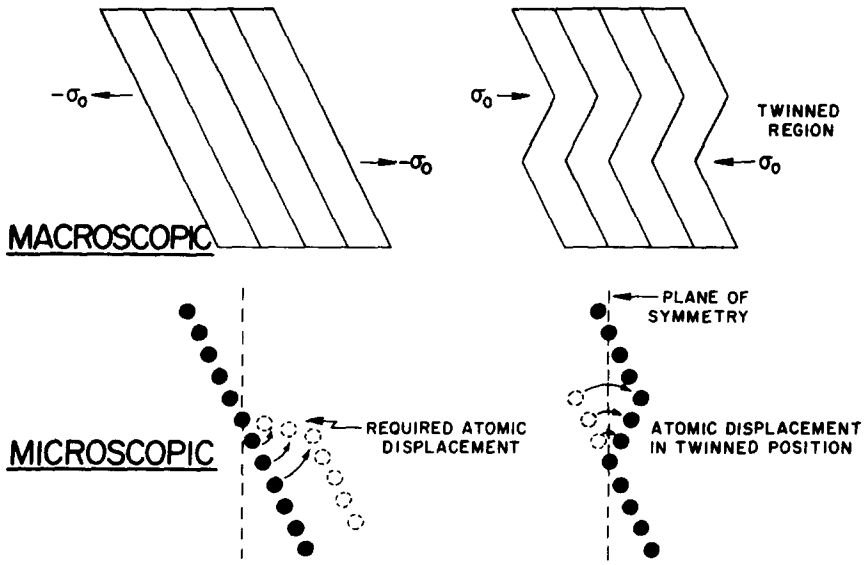


FIG. 21. Schematic illustration of the twinning process. The left-hand scheme illustrates that no twin positions of the atoms exist which could accommodate the stress $-\sigma_0$.

tion are included. The formal interpretation of the resonance curve and automodulation data by the inclusion of the half harmonic in the solution of the differential equation of motion and the necessary choice of an antisymmetric deformation potential are thus consistent with the known facts of twinning.

The stresses arising in the vicinity of twins can be accommodated elastically if the twins are small enough in size, a situation commonly referred to as microtwinning. In this case twinning can be expected to occur in a reversible fashion, i.e., it can be investigated by a periodic technique such as the one used in this study. The reproducibility of the data indicates that microtwinning occurs in the course of the reed oscillations. The resonance curves of the reed are, however, not exactly the same before and after a set of automodulation data were taken. This is shown in Fig. 18. It can be expected that the resonance curve changes gradually as the automodulation data are taken, which is another reason for the above mentioned differences between the experimental and computer modelled data. The amplitudes and frequencies of the automodulations must then be expected to change in the course of time, as is evident in Fig. 17. It may be conjectured that during this long time, the dynamical strain field around the microtwins changes as it is known that magnesium can recover at room temperature.[23] It is interesting that the resonance curve taken after the observation of the automodulation data reverts, in one day at 22 °C, the temperature of the experiment, to the one observed before the automodulation data were taken.

From a metallurgical point of view, the most interesting piece of information is the relaxation time $\tau = 10\omega_0^{-1}$ following from the comparison of Figs. 7 and 15. Since it describes the automodulation, i.e., exclusively the nonlinear aspect of the internal friction data, it must be attributed to the twinning process. Considering the case in which the eigenfrequency is 72 Hz, it follows that the relaxation of twinning of the magnesium sample under investigation is $\tau = 22$ msec, a surprisingly long time.

The relaxation for twinning $\tau$ may be considered to be the sum of a nucleation time $\tau_n$ and a settling time $\tau_s$. In terms of lattice waves, the former is given by the time it takes to build a large lattice wave required to displace the lattice atoms to their twinned positions. The latter, analogously, is determined by the time it takes for this lattice wave to decay. The settling time is determined by the thermoelastic damping.[24] It will be of the order of $\tau_s \approx a^2/D$, where $a$ is the typical dimension of a microtwin and $D$ is the thermal diffusivity. With the values of $a \approx 10^{-5}$ cm and $D = 0.1$ cm$^2$ sec$^{-1}$ it follows that $\tau_s = 10^{-9}$ sec, i.e., $\tau_s$ is not time controlling, rather $\tau_n$. Large amplitude lattice waves occur in the vicinity of lattice point defects particularly when the point defect is in a thermally activated state, i.e., is diffusing through the lattice. If this happens, the nucleation time of stress induced twinning is given by the time required for the deformation to reach a thermally activated state, i.e., by its diffusion time. This time can be very long. Therefore, it is suggested that the relaxation time of stress induced twinning determined in this study represents the characteristic time of a diffusional jump of a defect. It follows that the nucleation time of stress induced twinning is given by the relaxation time of reorientation of the defect in question. The nature of the defect controlling stress induced twinning in the magnesium sample used in this study is not known. There are, however, indications that the reorientation of oxygen can trigger twinning in zirconium.[25]

## ACKNOWLEDGMENT

The support of the National Science Foundation is gratefully acknowledged.

## APPENDIX A: COMPLETE EXPRESSIONS FOR THE FUNCTIONS $a_i$ AND $\theta_i$

The functions $a_i$ and $\theta_i$ appearing in Eqs. (13) and (14) are given below for the two cases of antisymmetric and symmetric deformation potentials.

### I. Antisymmetrical potential

$$a_1 = -(C_{u2} - 1) - 2C_{u3}a - 7C_{u5}(a^3 + 3aE'^2),$$
$$a_2 = (C_{u2} - 1)b/a + 4C_{u3}E' + 7C_{u5}(a^2E' + 3E'^3),$$
$$a_3 = 2C_{r3}E' + (7/2)C_{r5}(2a^2E' + 3E'^3),$$
$$\theta_1 = C_{r3}a + (7/2)C_{r5}(a^3 + 3aE'^2),$$
$$\theta_2 = -2C_{r3}E' - (7/2)C_{r5}(4a^2E' + 3E'^3),$$
$$\theta_3 = (C_{u2} - 1)b/a + 4C_{u3}E' + 7C_{u5}(2a^2E' + 3E'^3).$$

### II. Symmetrical potential

$$a_1 = -(C_{u2} - 1) - (45/16)C_{u4}(a^2 + 2b^2) - (131/64)C_{u6}(a^4 + 3a^2b^2 + 3b^4),$$
$$a_2 = (C_{u2} - 1)b/a + (45/16)C_{u4}(3ab + b^3/a) + (131/64)C_{u6}(3a^3b + 9ab^3 + b^5/a),$$
$$a_3 = (135/16)C_{r4}(ab + b^3/a) + (655/64)C_{r6}(a^3b + 3ab^3 + b^5/a),$$
$$\theta_1 = (135/16)C_{r4}(a^2 + 2b^2) + (655/128)C_{r6}(2a^4 + 12a^2b^2 + 3b^4),$$
$$\theta_2 = -(135/16)C_{r4}(3ab + b^3/a) - (655/64)C_{r6}(5a^3b + 9ab^3 + b^5/a),$$
$$\theta_3 = (C_{u2} - 1)b/a + (45/16)C_{u6}(ab + b^3/a) + (131/64)C_{u6}(a^3b + 3ab^3 + b^5/a).$$

## APPENDIX B: EXPRESSIONS REPRESENTING THE TERMS THAT APPEAR IN EQ. (16) USED FOR RESONANCE CALCULATIONS

$$A = [a_3 + \theta_3(\omega_0\tau)^2] + [(\theta_2 + a_2)\omega_0\tau]^2,$$
$$B = -a_1\theta_3^2(\omega_0\tau)^4 + \theta_1a_3^2 + (\theta_1 - a_1)a_3\theta_3(\omega_0\tau)^2 + \theta_1a_2^2(\omega_0\tau)^2 - a_1\theta_2^2(\omega_0\tau)^2 + (\theta_1 - a_1)\theta_2a_2(\omega_0\tau)^2,$$
$$C = [a_1\theta_3(\omega_0\tau)^2 - \theta_1a_3]^2 + [(\theta_1a_2 - a_1\theta_2)(\omega_0\tau)^2]^2 - [a_2\theta_3(\omega_0\tau)^2 - a_3\theta_2]^2.$$


[1] See, for example, R. Gibala and C. A. Wert, in *Diffusion in Body Centered Cubic Metals* (ASM, Metals Park, Ohio, 1965).
[2] See, for example, the work of the Grenoble group reported in the International Conferences on Vacancies and Interstitials in Metals held in Jülich 1968, Birmingham 1971, Gatlinburg 1974, and Argonne 1977.
[3] See, for example, R. Gibala and C. A. Wert, Acta Metall. **14**, 1095 (1966).
[4] See, for example, J. C. Swartz, J. W. Shilling, and A. J. Schwoeble, Acta Metall. **16**, 1359 (1968).
[5] C. Zener, *Elasticity and Anelasticity of Metals* (University of Chicago, Chicago, 1948).
[6] A. S. Nowick and W. R. Heller, Adv. Phys. **12**, 251 (1963).
[7] A. S. Nowick and W. R. Heller, Adv. Phys. **14**, 101 (1965).
[8] A. S. Nowick, J. Phys. Chem. Solids **31**, 1819 (1970).
[9] D. S. Richter and A. S. Nowick, Scripta Metall. **10**, 1043 (1976).
[10] F. Larché and J. W. Cahn, Acta Metall. **26**, 53 (1978).
[11] M. Wuttig and T. Suzuki, Acta Metall. **27**, 755 (1979).
[12] M. Wuttig and T. Suzuki, Proceedings of the International Conference on Ultrasonic Attenuation and Internal Friction, Lausanne, Switzerland (1981).
[13] K. N. Tong, *Theory of Mechanical Vibration* (Wiley, New York, 1960).
[14] N. Minorsky, *Nonlinear Oscillations* (Van Nostrand, New York, 1962).
[15] P. Glansdorff and I. Prigogine, *Thermodynamic Theory of Structure, Stability and Fluctuations* (Wiley, New York, 1971).
[16] A. Aning, T. Suzuki, and M. Wuttig, Scripta Metall. **16**, 189 (1982).
[17] M. Wuttig, A. Aning, and T. Suzuki, Scripta Metall. **15**, 1237 (1981).
[18] S. Takahaski, J. Appl. Phys. **23**, 866 (1952).
[19] I. A. Ritchie and A. Atrens (private communication).
[20] W. J. Baxter and J. Wilks, Philos. Mag. **7**, 427 (1962).
[21] W. de Jonghe, R. DeBatist, L. Delaey, and M. DeBonte, in *Shape Memory Effects in Alloys*, edited by J. Perkins (Plenum, New York, 1975).
[22] R. E. Reed-Hill, *Physical Metallurgy Principles* (Van Nostrand, New York, 1973).
[23] A. G. Guy and J. J. Hren, *Elements of Physical Metallurgy*, 3rd ed. (Addison-Wesley, Reading, Mass., 1974).
[24] A. S. Nowick and B. S. Berry, *Anelastic Relaxation in Crystalline Solids* (Academic, New York, 1972).
[25] I. G. Ritchie and K. W. Sprungmann, Atomic Energy of Canada Ltd., Report No. 6810 (1981).